Eur. Phys. J. C 4, 339–349 (1998)
DOI 10.1007/s100529800754

THE EUROPEAN PHYSICAL JOURNAL C
© Springer-Verlag 1998

Calculations of one-loop supersymmetric corrections to large-E_T jet cross sections

John Ellis[1], Douglas A. Ross[2]

[1] Theoretical Physics Division, CERN, CH-1211 Geneva 23, Switzerland
[2] Physics Department, University of Southampton, Southampton SO17 1BJ, United Kingdom

Received: 18 August 1997 / Published online: 20 February 1998

Abstract. We have calculated the one-loop supersymmetric corrections to the $2 \to 2$ parton scattering subprocesses $\bar{q}q \to \bar{q}q, \bar{q}q \to gg, gq \to gq$ and $gg \to gg$, including form-factor corrections and box diagrams with internal squarks and gluinos of arbitrary mass. In general, these exhibit cusps at the corresponding direct-channel sparticle thresholds. We use these calculations to make numerical estimates of the possible threshold effects at the Fermilab Tevatron collider and at the LHC, which depend on the rapidity range selected, but can be as large as a few percent. These effects are diluted in the integrated large-E_T cross section, where they are negative.

1 Introduction

Large samples of inclusive hadronic jets are available now from the Fermilab Tevatron collider, and will become available from the LHC in the future. These offer the prospects of precision tests of QCD, which is of interest and importance in its own right. Moreover, as the dynamics of QCD is better understood, it becomes a sharper tool for probing possible physics beyond the Standard Model. Complete calculations of jet physics to next-to-leading order in perturbation theory exist in pure QCD [1,2]. However, this may not be sufficient for precision physics at an exploratory machine that opens up a new energy range where there may be thresholds for new physics. For instance, the Fermilab Tevatron collider has already crossed the threshold for $\bar{t}t$ production, and either it or the LHC should cross the threshold for squark and gluino production. In the neighbourhood of, and beyond, the threshold for such new heavy strongly-interacting particles, their virtual effects should be included in a complete treatment of one-loop perturbative QCD effects.

Our attention was drawn to this problem by recent measurements of large-E_T jet cross sections at the Tevatron collider [3,4], some of which exhibited a *prima facie* discrepancy with predictions based on the parton distribution functions available previously. Clearly there are uncertainties in these distributions [5,6], which are not (yet) calculable from first principles, and it has been argued in particular [5] that reasonable uncertainties in the gluon distribution could accommodate simultaneously both the CDF [3] and D0 [4] jet measurements. However, it has also been argued that strong-interaction threshold effects could be significant [7,8], with emphasis placed on the possible importance of the sparticle threshold [8]. One might consider whether such a threshold effect could provide an alternative signature for sparticles, if their decays differ from those anticipated in conventional direct searches. Even if one does not expect the sparticle threshold to be very important, it is clearly desirable to have an exact one-loop treatment of it, just as one-loop sparticle corrections are known and used in the analysis of precision electroweak physics at and around the Z^0 peak [9].

We have undertaken detailed calculations of such corrections in the Minimal Supersymmetric extension of the Standard Model (MSSM), and published first results [10]. We found that there could be threshold structures of the order of a few % in the cross sections for individual parton-parton scattering subprocesses when one-loop corrections were included. However, these were of the wrong shape and of insufficient magnitude to make a significant contribution to the resolution of the CDF large-E_T conundrum [3]. The purpose of this paper is to complete the analysis of [10], presenting more details of the calculations, presenting the one-loop corrections to all partonic subprocesses, including box diagrams and the $gg \to gg$ subprocess, which were not included in [10], and combining our calculations in a complete one-loop numerical analysis[1] of jet cross sections at Fermilab and the LHC, including the appropriate convolutions over all the contributing parton-parton scattering subprocesses.

The layout of this paper is as follows. In Sect. 2 we present details of our results [10] for the calculations of the one-loop corrections to the partonic subprocesses arising from the form-factor corrections to the triple-gluon vertex and the quark-quark-gluon vertex, which include self-

[1] Numerical results of such a study have also been published in [11]

energy corrections due to squarks[2] and gluinos. We comment on various consistency checks on our calculations, demonstrating in particular cancellations between different diagrams associated with Ward identities, and remaining logarithmic singularities that reflect the expected running of the strong coupling α_s above the supersymmetric threshold. Section 3 contains a similar analysis of one-loop box diagrams, including a number of further consistency checks. Numerical results are presented in Sect. 4, including the convolutions with parton distribution functions which are appropriate for the analysis of jet cross sections at the Fermilab Tevatron collider when $E_T \simeq m \equiv m_s = m_g = 200$ GeV (where $m_{s,g}$ denote the squark and gluino masses), and at the LHC when $E_T \simeq m = 1$ TeV. Section 5 summarizes our conclusions from our calculations. In the appendix we list the Veltman-Passarino [12] functions, in terms of which our results are displayed.

2 Form-factor corrections

In this section present the form-factor corrections for the partonic subprocesses

$$q(p_1) + \bar{q}(p_2) \to q(p_3) + \bar{q}(p_4) \tag{2.1}$$

$$q(p_1) + \bar{q}(p_2) \to g(p_3) + g(p_4) \tag{2.2}$$

$$g(p_1) + g(p_2) \to g(p_3) + g(p_4). \tag{2.3}$$

calculated using the $\overline{MS}$ prescription. The form factors for all other partonic subprocesses can be obtained from these by exploiting crossing symmetry.

The contribution to the amplitude for the subprocess (2.1) from all diagrams except box graphs may be written in the general form

$$\frac{4\pi i\alpha_s}{s}\bar{v}(p_4)F_{qqg}(s)\gamma^\mu\tau^a u(p_3)\,\bar{v}(p_2) \times \quad F^{qqg}(s)\gamma^\mu\tau^a u(p_1), \tag{2.4}$$

where τ^a is the generator of colour $SU(3)$ in the defining representation, and $F_{qqg}(s)$ is a form factor for the quark-quark-virtual-gluon vertex. The tree-level amplitude is obtained by replacing this form factor by unity. The one-loop corrections to this form factor from internal squarks and gluinos come from the diagrams shown in Fig. 1a,b,g,h, and give a contribution to F_{qqg} of the form

$$\begin{aligned}\Delta F_{qqg} = \frac{\alpha_s}{4\pi}\Bigg\{ & 4\left(C_F - \frac{C_A}{2}\right)C_{24}(\{1\}) \\ & + C_A\Bigg[-\frac{1}{2} + 2C_{24}(\{2\}) - m_g^2 C_0(\{2\}) \\ & + s\left(C_{23}(\{2\}) + C_{12}(\{2\})\right) \\ & - \frac{1}{3}\left(\frac{2m_g^2}{s} + 1\right)\left(B_0(\{1\}) + 1\right) + \frac{2}{3s}A(m_g) + \frac{4}{9}\Bigg] \\ & - \frac{1}{3}T_R\Bigg[\left(1 - \frac{4m_s^2}{s}\right)\left(B_0(\{2\}) + 1\right) \\ & + \frac{4}{s}A(m_s) - \frac{1}{3}\Bigg]\Bigg\},\end{aligned} \tag{2.5}$$

where the Veltman-Passarino (VP) functions [12] C_i, B_0 are given in the appendix. They are calculated in $n = 4-2\epsilon$ dimensions, and the arguments $\{1\}$, $\{2\}$ are defined by

$$\begin{aligned} C_i(\{1\}) &= C_i(s, m_s, m_g, m_s), \\ C_i(\{2\}) &= C_i(s, m_g, m_s, m_g), \\ B_0(\{1\}) &= B_0(s, m_g, m_g), \end{aligned}$$

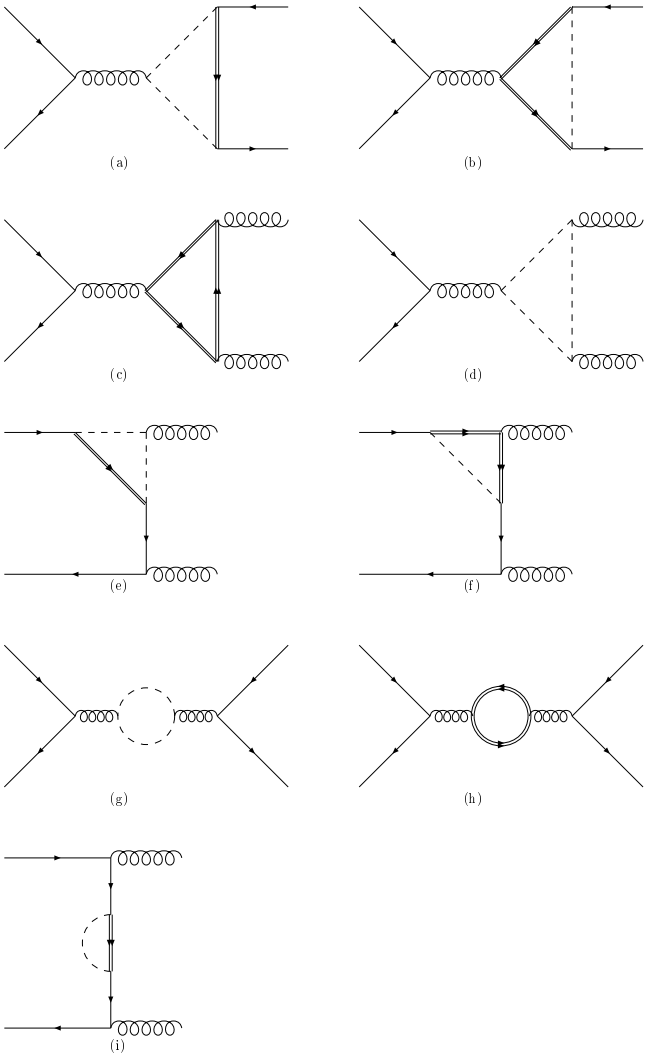

Fig. 1. One-loop Feynman diagrams involving virtual sparticles in the MSSM for **a**,**b** the virtual-$g\bar{q}q$ vertex, **c**,**d** the virtual-ggg vertex, **e**,**f** the virtual-$q\bar{q}g$ vertex, **g**,**h** the gluon self energy, and **i** the quark self energy. Here and in subsequent figures of Feynman diagrams, the *broken lines* represent squarks and the *double solid lines* represent gluinos

[2] We assume for simplicity that all the relevant left- and right-handed squarks have equal masses. This means that our results should not be assumed to apply to processes involving both sbottom and stop squarks

$$B_0(\{2\}) = B_0(s, m_s, m_s), \tag{2.6}$$

where m_s and m_g are the squark and gluino masses, respectively. For the unsubtracted correction to the form factor, we must add to (2.5) the pole term

$$-C_F \frac{\alpha_s}{\epsilon}, \tag{2.7}$$

which arises from the wave-function renormalization of the external quarks, and cancels the pole part of (2.5) proportional to C_F, as required by the abelian Ward identity. Substituting the ultraviolet-divergent functions by their pole parts, given in (A.13-A.15), we see that the poles from the one-particle irreducible vertex corrections shown in Figs. 1a,b) which are proportional to C_A also cancel between the two diagrams. The the remaining divergences come from the functions B_0, which contribute to the extra renormalization of the strong coupling due to supersymmetric particles, namely

$$-\frac{\alpha_s}{12\pi\epsilon}\left(C_A + T_R\right), \tag{2.8}$$

and arise from the gluon self-energy contributions shown in Figs. 1g,h).

Once this renormalization has been effected, the finite form factor is given by (2.5), with the divergent functions B_0 and C_{24} understood to have been subtracted using the $\overline{MS}$ prescription. The resulting contribution to the form factor vanishes in the limit $s \to 0$ when we set $m_s = m_g = m$. In the limit $s \ll m^2$ the form-factor correction is given by the following simple expression:

$$\lim_{s \ll m^2} \Delta F_{qqg} \to \frac{\alpha_s}{4\pi}\left\{\frac{C_F}{12} + \frac{C_A}{60} - \frac{T_R}{30}\right\}\frac{s}{m^2}. \tag{2.9}$$

which is $\mathcal{O}(0.1(s/m^2))\%$. This and other form-factor corrections are actually numerically considerably larger when $s \sim m^2$ [10], as we shall see later.

The amplitude for the process (2.2), again omitting for the moment box diagrams, may be written as

$$\begin{aligned}-i4\pi\alpha_s\epsilon_3^\nu\epsilon_4^\rho \Bigg\{ & \frac{1}{t}\bar{v}(p_2)\tau^{a_4}\tau^{a_3} \\ & \times F^\rho_{gqq}(p_1 - p_3)(\not{p}_1 - \not{p}_3)F^\nu_{gqq}(p_1 - p_3)u(p_1) \\ & + \frac{1}{u}\bar{v}(p_2)\tau^{a_3}\tau^{a_4} \\ & \times F^\nu_{gqq}(p_1 - p_4)(\not{p}_1 - \not{p}_4)F^\rho_{gqq}(p_1 - p_4)u(p_1) \\ & - \frac{1}{s}\bar{v}(p_2)\left[\tau^{a_3}, \tau^{a_4}\right] \\ & \times F_{qqg}(s)\gamma^\mu V_3^{\mu\nu\rho}(p_3, p_4)u(p_1)\Bigg\}, \end{aligned} \tag{2.10}$$

where ϵ_3, ϵ_4 are the polarization vectors of the external gluons with momenta p_3, p_4, whose colours are a_3, a_4, respectively.

The quantity $F^\mu_{gqq}(q)$ is the form factor for the gluon-quark-virtual-quark vertex, which at the tree level is simply γ^μ. The diagrams contributing to the corrections to this form factor which involve internal squarks and gluinos are shown in Fig. 1e,f,i, and give a contribution

$$\begin{aligned}\Delta F^\mu_{gqq}(q) = \frac{\alpha_s}{4\pi}\Bigg\{ & \left(4C_F - 2C_A\right)\left[C_{24}(\{4\})\gamma^\mu + \left(C_{22}(\{4\})\right.\right. \\ & \left. - C_{23}(\{4\})\not{q}q^\mu\right] + C_A\Big[\Big(2C_{24}(\{5\}) - \frac{1}{2} - m_g^2 C_0(\{5\}) \\ & - q^2\left(C_{22}(\{5\}) + C_{23}(\{5\})\right)\Big)\gamma^\mu + 2C_{23}(\{5\})\not{q}q^\mu\Big] \\ & - \frac{C_F}{2}\Bigg[\frac{(m_g^2 - m_s^2 + q^2)}{q^2}B_0(q^2, m_s, m_g) \\ & - \frac{1}{q^2}\left(A(m_g) - A(m_s)\right)\Bigg]\gamma^\mu\Bigg\}, \end{aligned} \tag{2.11}$$

where the arguments $\{4\}$, $\{5\}$ are given by

$$\begin{aligned} C_i(\{4\}) &= C_i(q^2, m_s, m_s, m_g), \\ C_i(\{5\}) &= C_i(q^2, m_g, m_g, m_s). \end{aligned} \tag{2.12}$$

To obtain the unsubtracted form factor, we must add a pole term

$$-\frac{\alpha_s}{4\pi\epsilon}\left(\frac{C_F}{2} + \frac{C_A}{3} + \frac{T_R}{3}\right), \tag{2.13}$$

which arises from the wave-function renormalizations of the external quark and gluon legs. Once this is included, we notice that again the abelian pole term proportional to C_F cancels. The remaining pole term is given by (2.8), and is absorbed by the renormalization of the strong coupling. After this renormalization, and setting $m_s = m_g = m$, we find that for $q^2 \ll m^2$

$$\begin{aligned}\lim_{q^2 \ll m^2} \Delta F^\mu_{gqq}(q) \to \frac{\alpha_s}{4\pi}\Bigg\{ & C_A\left[\frac{q^2}{4m^2}\gamma^\mu - \frac{1}{3m^2}\not{q}q^\mu\right] \\ & + \frac{C_F}{6m^2}\not{q}q^\mu\Bigg\} \end{aligned} \tag{2.14}$$

which is $\mathcal{O}(1(q^2/m^2)\%$.

The three-gluon vertex function $V_3^{\mu\nu\rho}(p_3, p_4)$ may be written as

$$\begin{aligned} V_3^{\mu\nu\rho}(p_3, p_4) = & -2g^{\nu\rho}p_4^\mu F_1(s) + 2g^{\mu\rho}p_4^\nu F_2(s) \\ & -2g^{\mu\nu}p_3^\rho F_2(s) + p_4^\nu p_3^\rho p_4^\mu F_3(s), \end{aligned} \tag{2.15}$$

where $s = 2p_3 \cdot p_4$. At the tree level, the form factors F_1, F_2 take the value unity, whereas F_3 is zero. The irreducible one-loop contributions from squark and gluino loops to these form factors are are shown in Fig. 1c,d, and are given by

$$\begin{aligned}\Delta F_1(s) = \frac{\alpha_s}{4\pi}\Bigg\{ C_A\Bigg[& -\frac{2}{3} - m_g^2\left(C_0(\{6\}) - C_{11}(\{6\})\right. \\ & + C_{12}(\{6\})) + s\left(C_{12}(\{6\}) + C_{22}(\{6\})\right. \\ & - C_{33}(\{6\}) + C_{34}(\{6\})) - 2C_{35}(\{6\}) \\ & + 2C_{36}(\{6\}) + 2C_{24}(\{6\}) - \frac{1}{3}\left(\frac{2m_g^2}{s} + 1\right) \end{aligned}$$

$$\times (B_0(\{1\})+1) + \frac{2}{3s}A(m_g) + \frac{4}{9}\Bigg]$$
$$+T_R\Bigg[8C_{36}(\{7\}) - 8C_{35}(\{7\})$$
$$-\frac{1}{3}\left(1-\frac{4m_s^2}{s}\right)(B_0(\{2\})+1)$$
$$-\frac{4}{3s}A(m_s)+\frac{1}{9}\Bigg]\Bigg\}, \qquad (2.16)$$

$$\Delta F_2(s) = \frac{\alpha_s}{4\pi}\Bigg\{C_A\Bigg[-\frac{2}{3} - m_g^2\left(C_0(\{6\}) - C_{12}(\{6\})\right)$$
$$-s\left(C_{22}(\{6\}) + C_{34}(\{6\})\right)$$
$$-2C_{36}(\{6\}) + 2C_{24}(\{6\})$$
$$-\frac{1}{3}\left(\frac{2m_g^2}{s}+1\right)(B_0(\{1\})+1) + \frac{2}{3s}A(m_g) + \frac{4}{9}\Bigg]$$
$$+T_R\left[-8C_{36}(\{7\}) - \frac{1}{3}\left(1-\frac{4m_s^2}{s}\right)\right.$$
$$\left.\times\,(B_0(\{2\})+1) - \frac{4}{3s}A(m_s) + \frac{1}{9}\right]\Bigg\}, \qquad (2.17)$$

$$\Delta F_3(s) = \frac{2\alpha_s}{\pi}\Bigg\{C_A\left[C_{22}(\{6\}) - C_{23}(\{6\}) - C_{33}(\{6\})\right.$$
$$\left.+C_{34}(\{6\})\right] + 2T_R\left[C_{23}(\{7\}) - C_{22}(\{7\})\right.$$
$$\left.+C_{33}(\{7\}) - C_{34}(\{7\})\right]\Bigg\}, \qquad (2.18)$$

where the arguments $\{6\}$, $\{7\}$ are given by

$$C_i(\{6\}) = C_i(s, m_g, m_g, m_g),$$
$$C_i(\{7\}) = C_i(s, m_s, m_s, m_s). \qquad (2.19)$$

To obtain the unsubtracted form factor, we must add a pole term

$$-\frac{\alpha_s}{4\pi\epsilon}\left(\frac{2C_A}{3}+\frac{2T_R}{3}\right), \qquad (2.20)$$

which arises from the wave-function renormalizations of the external gluon legs as shown in Fig. 1g,h, leaving a pole term equal to (2.8). After renormalization and setting $m_s = m_g = m$, we find that for $s \ll m^2$

$$\lim_{s\ll m^2}\Delta F_1(s) \to \frac{\alpha_s}{48\pi}C_A\frac{s}{m^2} \qquad (2.21)$$

$$\lim_{s\ll m^2}\Delta F_2(s) \to \frac{\alpha_s}{60\pi}\left(C_A+\frac{T_R}{2}\right)\frac{s}{m^2} \qquad (2.22)$$

$$\lim_{s\ll m^2}\Delta F_3(s) \to \frac{\alpha_s}{60\pi}\left(C_A - 2T_R\right)\frac{1}{m^2} \qquad (2.23)$$

which are comparable in magnitude to the low-energy expansions of the previous form factors. Apart from some minor differences, the low-energy expansions of our results (2.9, 2.14, 2.21, 2.22, 2.23) confirm the general magnitudes of the below-threshold corrections found in [8].

Finally, we can use V_3 to write down the amplitude for process (2.3) excluding the box diagrams which contribute to the renormalization of the four-gluon coupling, which we postpone until the next section:

$$i\frac{4\pi\alpha_s}{s}\epsilon_1^\mu\epsilon_2^\nu\epsilon_3^\rho\epsilon_4^\sigma f^{a_1a_2b}f^{a_3a_4b}V_3^{\tau\mu\nu}(p_1,p_2)V_3^{\tau\rho\sigma}(p_3,p_4)$$
$$+\text{ permutations }\{2,3,4\}, \qquad (2.24)$$

where ϵ_1, ϵ_2 are the polarization vectors of the incoming gluons with momenta p_1, p_2, whose colours are a_1, a_2, respectively, and ϵ_3, ϵ_4 are the polarization vectors of the outgoing gluons with momenta p_3, p_4, whose colours are a_3, a_4, respectively. The notation "permutations $\{2,3,4\}$" means permutations over the momenta, polarization vectors and colours of gluons 2,3,4.

3 Box diagrams

For the box diagrams we need the four-point VP functions D_i [12] listed in the appendix in (A.8) to (A.12).

The box diagrams for the process (2.1), shown in Fig. 2, give the following contribution to the amplitude:

$$2iC_A\alpha_s^2\left\{D_2(t,u,m_s,m_g,m_s,m_g,\mu,\nu)\left[A_{VV}^{\mu\nu}+A_{AA}^{\mu\nu}\right]\right.$$
$$\left.+m_g^2D_0(t,u,m_s,m_g,m_s,m_g)\left[A_{SS}+A_{PP}\right]\right\}$$
$$+(t\leftrightarrow u) \qquad (3.1)$$

where

$$A_{VV}^{\mu\nu} = \bar v(p_4)\gamma^\mu\tau^a v(p_2)\ \bar u(p_3)\gamma^\nu\tau^a u(p_1)$$
$$A_{AA}^{\mu\nu} = \bar v(p_4)\gamma^\mu\gamma^5\tau^a v(p_2)\ \bar u(p_3)\gamma^\nu\gamma^5\tau^a u(p_1)$$
$$A_{SS} = \bar v(p_4)\tau^a v(p_2)\ \bar u(p_3)\tau^a u(p_1)$$
$$A_{PP} = \bar v(p_4)\gamma^5\tau^a v(p_2)\ \bar u(p_3)\gamma^5\tau^a u(p_1)$$

The second graph in Fig. 2 arises from the Majorana nature of the internal gluino lines, which permits them to propagate both along and against the flow of the quark fermion number.

The box diagrams for the process (2.2) are shown in Fig. 3. Figure 3a gives a contribution

$$-2i\alpha_s^2\epsilon_3^\nu\epsilon_4^\sigma\left\{\left[D_3(t,u,m_s,m_g,m_g,m_g,\mu,\rho,\tau)\right.\right.$$
$$\left.+(p_1-p_3)^\rho D_2(t,u,m_s,m_g,m_g,m_g,\mu,\tau)\right]B_{ab}^{\mu\nu\rho\sigma\tau}$$
$$+m_g^2\left[D_1(t,u,m_s,m_g,m_g,m_g,\mu)\left(B_{ab}^{\nu\mu\sigma}+B_{ab}^{\mu\nu\sigma}+B_{ab}^{\nu\sigma\mu}\right)\right.$$
$$\left.\left.+(p_1-p_3)^\mu D_0(t,u,m_s,m_g,m_g,m_g)B_{ab}^{\nu\mu\sigma}\right]\right\}$$
$$+(3\leftrightarrow 4), \qquad (3.2)$$

where the tensors B are defined as

$$B_{ab}^{\mu_1\cdots\mu_n} = \bar v(p_2)\left(\gamma^{\mu_1}\cdots\gamma^{\mu_n}\left[\tau^b,\tau^c\right]\left[\tau^a,\tau^c\right]\right)$$
$$\times u(p_1). \qquad (3.3)$$

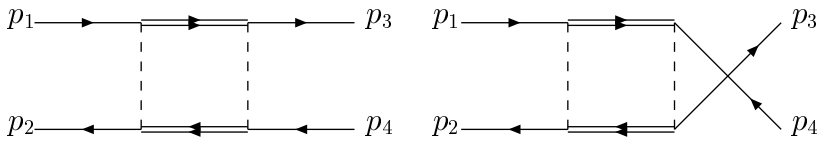

Fig. 2. Box diagrams for the process $q\,\bar{q} \to q\,\bar{q}$

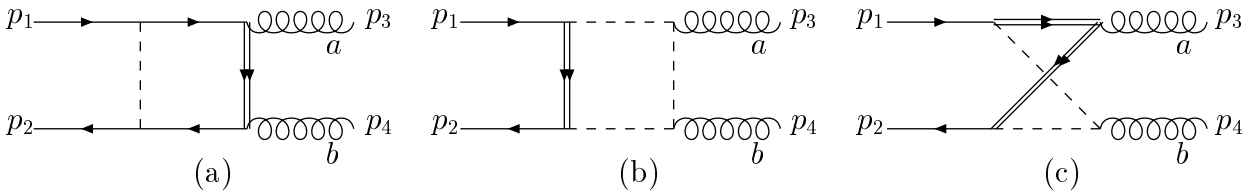

Fig. 3. Box diagrams for the process $q\,\bar{q} \to g\,g$

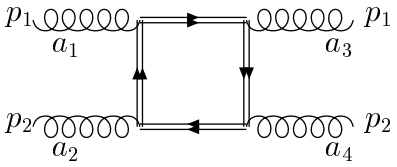

Fig. 4. Gluino box diagram for the process $g\,g \to g\,g$

Figure 3b gives a contribution

$$
\begin{aligned}
&-8i\alpha_s^2\epsilon_3^\nu\epsilon_4^\sigma\,\{\,D_3(t,u,m_g,m_s,m_s,m_s,\mu,\nu,\sigma)\\
&\quad+p_1^\nu D_2(t,u,m_g,m_s,m_s,m_s,\mu,\sigma)\\
&\quad+\,(p_1-p_3)^\sigma\,[\,D_2(t,u,m_g,m_s,m_s,m_s,\mu,\nu)\\
&\quad+p_1^\nu D_1(t,u,m_g,m_s,m_s,m_s,\mu)]\}\\
&\quad\times\bar{v}(p_2)\left(\gamma^\mu\tau^c\tau^b\tau^a\tau^c\right)u(p_1)\;+(3\leftrightarrow 4)
\end{aligned}
\tag{3.4}
$$

Figure 3c gives a contribution

$$
\begin{aligned}
&-4i\alpha_s^2\epsilon_3^\nu\epsilon_4^\sigma\,\{\,[\,D_3(t,s,m_s,m_g,m_g,m_s,\mu,\rho,\sigma)\\
&\quad+(p_1-p_3)^\mu D_2(t,s,m_s,m_g,m_g,m_s,\rho,\sigma)]\;B'^{\mu\nu\rho}_{ab}\\
&\quad+m_g^2\,D_1(t,s,m_s,m_g,m_g,m_s,\sigma)B'^{\nu}_{ab}\,\}\\
&\quad+(3\leftrightarrow 4),
\end{aligned}
\tag{3.5}
$$

where the tensors B' are defined by

$$
B'^{\mu_1\cdots\mu_n}_{ab} = if^{dac}\,\bar{v}(p_2)\left(\gamma^{\mu_1}\cdots\gamma^{\mu_n}\tau^c\tau^b\tau^d\right)u(p_1). \tag{3.6}
$$

and the notation $(3\leftrightarrow 4)$ means $(\epsilon_3\leftrightarrow\epsilon_4,\ p_3\leftrightarrow p_4,\ t\leftrightarrow u,\ a\leftrightarrow b)$.

The contributions to the process (2.3) from box diagrams are shown in Fig. 4 (for an internal gluino loop) and Fig. 5 (for an internal squark loop). Also included in Fig. 5 are diagrams that involve the four-point coupling between gluons and squarks. Although these are not box diagrams, we include them here, because they do not contribute to the form factor for the triple-gluon vertex. The contribution to the amplitude from Fig. 4 is

$$
\begin{aligned}
&i\frac{\alpha_s^2}{2}G_1\,\{\,D_4(s,t,m_g,m_g,m_g,m_g,\mu,\nu,\rho,\sigma)\\
&\quad\times\mathrm{tr}\,(\not\epsilon_1\gamma^\mu\not\epsilon_4\gamma^\nu\not\epsilon_3\gamma^\rho\not\epsilon_2\gamma^\sigma)\\
&\quad+D_3(s,t,m_g,m_g,m_g,m_g,\mu,\nu,\rho)\\
&\quad\times[\,\mathrm{tr}\,(\not\epsilon_1\gamma^\mu\not\epsilon_4\not p_4\not\epsilon_3\gamma^\nu\not\epsilon_2\gamma^\rho)+\mathrm{tr}\,(\not\epsilon_1\gamma^\mu\not\epsilon_4\gamma^\nu\not\epsilon_3\gamma^\rho\not\epsilon_2\not p_1)\\
&\quad+\mathrm{tr}\,(\not\epsilon_1\gamma^\mu\not\epsilon_4\gamma^\nu\not\epsilon_3(\not p_1+\not p_2)\not\epsilon_2\gamma^\rho)\,]\\
&\quad+D_2(s,t,m_g,m_g,m_g,m_g,\mu,\nu)\\
&\quad\times[\,\mathrm{tr}\,(\not\epsilon_1\gamma^\mu\not\epsilon_4\not p_4\not\epsilon_3\gamma^\nu\not\epsilon_2\not p_1)+\mathrm{tr}\,(\not\epsilon_1\gamma^\mu\not\epsilon_4\not p_4\not\epsilon_3(\not p_1+\not p_2)\not\epsilon_2\gamma^\nu)\\
&\quad+\mathrm{tr}\,(\not\epsilon_1\gamma^\mu\not\epsilon_4\gamma^\nu\not\epsilon_3(\not p_1+\not p_2)\not\epsilon_2\not p_1)]\\
&\quad+D_1(s,t,m_g,m_g,m_g,m_g,\mu)\\
&\quad\times\mathrm{tr}\,(\not\epsilon_1\gamma^\mu\not\epsilon_4\not p_4\not\epsilon_3\,(\not p_1+\not p_2)\not\epsilon_2\not p_1)\\
&\quad+m_g^2D_2(s,t,m_g,m_g,m_g,m_g,\mu,\nu)\\
&\quad\times[16\epsilon_1^\mu\epsilon_3^\nu\epsilon_2\cdot\epsilon_4+16\epsilon_4^\mu\epsilon_2^\nu\epsilon_1\cdot\epsilon_3]\\
&\quad+m_g^2D_1(s,t,m_g,m_g,m_g,m_g,\mu)\\
&\quad\times[2\epsilon_4^\mu\mathrm{tr}\,(\not\epsilon_1\not\epsilon_3\,(\not p_1+\not p_2)\not\epsilon_2)\\
&\quad+2\epsilon_2^\mu\mathrm{tr}\,(\not\epsilon_1\not\epsilon_4\not p_4\not\epsilon_3)+2\epsilon_3^\mu\mathrm{tr}\,(\not\epsilon_1\not\epsilon_4\not\epsilon_2\not p_1)\\
&\quad+\mathrm{tr}\,(\not\epsilon_1\gamma^\mu\not\epsilon_4\not p_4\not\epsilon_3\not\epsilon_2)\\
&\quad+\mathrm{tr}\,(\not\epsilon_1\gamma^\mu\not\epsilon_4\not\epsilon_3\not\epsilon_2\not p_1)+\mathrm{tr}\,(\gamma^\mu\not\epsilon_1\not\epsilon_4\not\epsilon_3\,(\not p_1+\not p_2)\not\epsilon_2)\,]\\
&\quad+m_g^2D_0(s,t,m_g,m_g,m_g,m_g)\,[\mathrm{tr}\,(\not\epsilon_1\not\epsilon_4\not p_4\not\epsilon_3\,(\not p_1+\not p_2)\not\epsilon_2)\\
&\quad+\mathrm{tr}\,(\not\epsilon_1\not\epsilon_4\not\epsilon_3\,(\not p_1+\not p_2)\not\epsilon_2\not p_1)+\mathrm{tr}\,(\not\epsilon_1\not\epsilon_4\not p_4\not\epsilon_3\not\epsilon_2\not p_1)\,]\\
&\quad+m_g^4D_0(s,t,m_g,m_g,m_g,m_g)\mathrm{tr}\,(\not\epsilon_1\not\epsilon_4\not\epsilon_3\not\epsilon_2)\,\}\\
&\quad(+\text{ permutations }\{2,3,4\}),
\end{aligned}
\tag{3.7}
$$

where the colour factor G_1 is given by

$$
G_1 = f^{a_1ab}f^{a_2bc}f^{a_3cd}f^{a_4da}. \tag{3.8}
$$

In the interests of compactness, we have left this expression in terms of traces over γ matrices. The contribution from Fig. 5a is

$$
\begin{aligned}
&-32i\alpha_s^2G_2\,\epsilon_1^\mu\epsilon_2^\nu\epsilon_3^\rho\epsilon_4^\sigma\,\{\,D_4(s,t,m_s,m_s,m_s,m_s,\mu,\nu,\rho,\sigma)\\
&\quad+p_1^\nu D_3(s,t,m_s,m_s,m_s,m_s,\mu,\rho,\sigma)\\
&\quad+(p_1+p_2)^\rho\,D_3(s,t,m_s,m_s,m_s,m_s,\mu,\nu,\sigma)\\
&\quad p_1^\nu(p_1+p_2)^\rho D_2(s,t,m_s,m_s,m_s,m_s,\mu,\sigma)\,\}\\
&\quad+\text{ permutations }\{2,3,4\}),
\end{aligned}
\tag{3.9}
$$

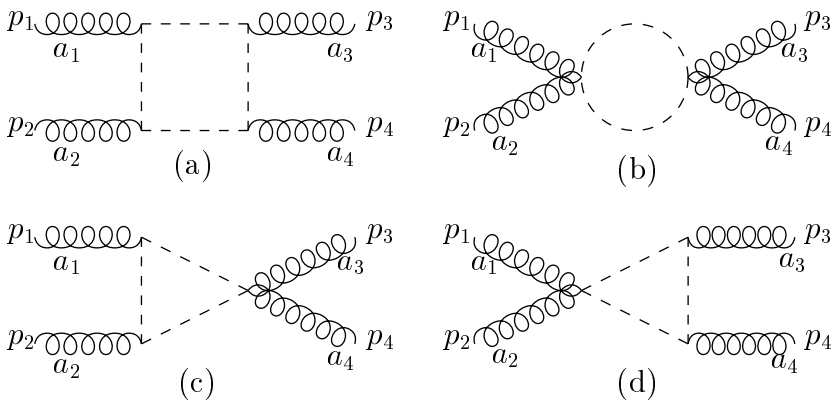

Fig. 5. a Squark box diagram and **b**,**c**,**d** diagrams involving quartic couplings that contribute to the process $g\,g \to g\,g$

where the colour factor G_2 is given by

$$G_2 = \mathrm{tr}\,(\tau^{a_1}\tau^{a_2}\tau^{a_3}\tau^{a_4}) \tag{3.10}$$

The contribution from Fig. 5b is

$$4i\alpha_s^2 G_3\,\epsilon_1\cdot\epsilon_4\,\epsilon_2\cdot\epsilon_3\;B_0(u,m_s,m_s) \tag{3.11}$$
$$(+\text{ permutations }\{2,3,4\}), \tag{3.12}$$

where the colour factor G_3 is given by

$$G_3 = \mathrm{tr}\left(\tau^{a_1}\tau^{a_2}\tau^{\{a_3}\tau^{a_4\}}\right) \tag{3.13}$$

The contribution from Fig, 5c is

$$-16i\alpha_s^2 G_3\,\epsilon_2\cdot\epsilon_3\,[\,C_{24}(u,m_s,m_s,m_s)\,\epsilon_1\cdot\epsilon_4 - C_{23}(u,m_s,m_s,m_s)\,p_4\cdot\epsilon_1\,p_1\cdot\epsilon_4] \quad (+\text{ permutations }\{2,3,4\}), \tag{3.14}$$

Finally, from Fig. 5d we get

$$-16i\alpha_s^2 G_3\,\epsilon_1\cdot\epsilon_4\,[\,C_{24}(u,m_s,m_s,m_s)\,\epsilon_2\cdot\epsilon_3 - C_{23}(u,m_s,m_s,m_s)\,p_3\cdot\epsilon_2\,p_2\cdot\epsilon_3] \quad (+\text{ permutations }\{2,3,4\}), \tag{3.15}$$

These contributions contain ultraviolet divergences, which are associated with the renormalization Z_4 of the four-point gluon vertex. Application of Ward identities tells us that the coefficient of the pole parts of the integrals should be given by the contribution $\Delta\beta_0$ to the β function, multiplied by the tree-level amplitude Γ_4 for the four-gluon coupling. In the above expressions, poles arise in the unsubtracted forms of the functions B_0, $C_{24}\,D_4$. Exploiting the pole parts displayed in the appendix in (A.14,A.15,A.18), and permuting the gluons 2,3,4, we arrive at a pole term

$$-\frac{\alpha_s}{4\pi\epsilon}\frac{2}{3}\,(C_A + T_R)\,\Gamma_4 = \frac{1}{\epsilon}\Delta\beta_0\Gamma_4, \tag{3.16}$$

as required.

In order to obtain the relevant contributions to the partonic cross sections, these contributions to amplitudes must be multiplied by the Hermitian conjugates of the corresponding tree-level amplitudes and summed (averaged) over final (initial) quark or gluon polarizations and colours. These tedious but straightforward manipulations are most conveniently performed using a fast algebraic manipulation package: we have used FORM.

Finally, we note that the box-diagram contributions for all other partonic subprocesses can be obtained from the above expressions by crossing symmetry.

4 Numerical results

We first present the results for the one-loop corrections to all the different parton-parton scattering cross sections shown in Fig. 6. These are for the simplified case $m_s = m_g = m$, although our analytical results apply for arbitrary ratios m_s/m_g. These extend and complete the analogous plots shown in [10], which did not include box diagrams, nor results for the subprocess $gg \to gg$. We already commented in [10] that we did not expect the box-diagram contributions to be numerically large, and this has been confirmed by our complete calculation.

We first note that, because these corrections to the cross sections are due to interferences between tree-level and one-loop amplitudes, they are not necessarily positive. In particular, processes which are dominated by the exchange of a parton in the t channel give a negative correction, and we see that the corrections in Fig. 6c,d,e are negative for $s \sim 4m^2$. We also note that each of the corrections exhibits a cusp at $\sqrt{s} = 2m$, creating a local maximum in the magnitude of the one-loop correction. This is largest for the subprocesses $q_j\bar{q}_j \to q_k\bar{q}_k$ and $q\bar{q} \to gg$ shown in Figs. 6a,b, which are unfortunately not dominant at the Fermilab Tevatron collider and the LHC. Next in magnitude is the $q_j g \to q_j g$ shown in Fig. 6, which is of greater experimental significance. The newly-calculated one-loop correction to the subprocess $gg \to gg$ shown in Fig. 6e is the smallest numerically.

We also note that each of the one-loop corrections grows logarithmically at large $s \gg m^2$. As was mentioned previously, some of this logarithmic behaviour is due to

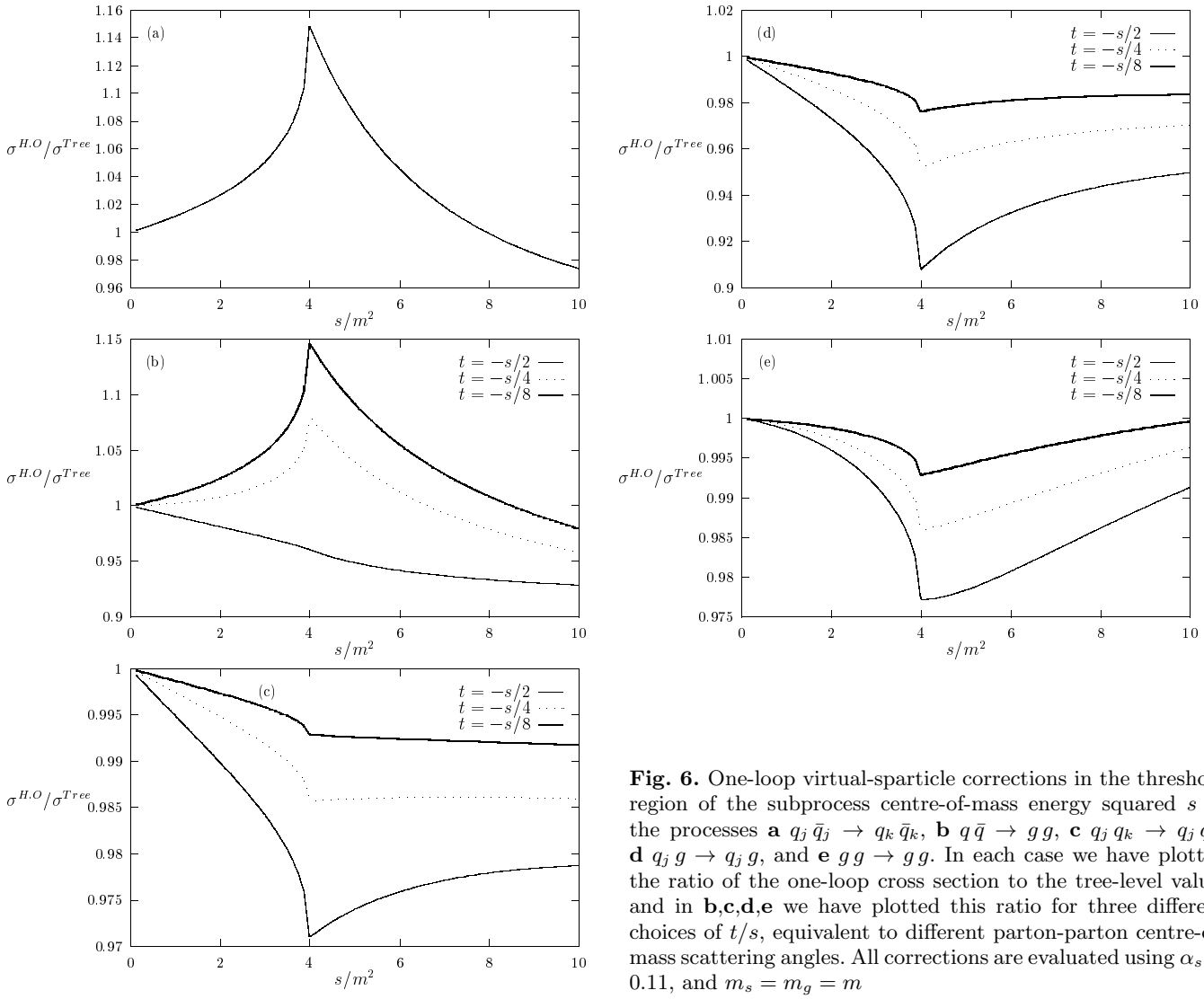

Fig. 6. One-loop virtual-sparticle corrections in the threshold region of the subprocess centre-of-mass energy squared s to the processes **a** $q_j\,\bar{q}_j \to q_k\,\bar{q}_k$, **b** $q\,\bar{q} \to g\,g$, **c** $q_j\,q_k \to q_j\,q_k$, **d** $q_j\,g \to q_j\,g$, and **e** $g\,g \to g\,g$. In each case we have plotted the ratio of the one-loop cross section to the tree-level value, and in **b**,**c**,**d**,**e** we have plotted this ratio for three different choices of t/s, equivalent to different parton-parton centre-of-mass scattering angles. All corrections are evaluated using $\alpha_s = 0.11$, and $m_s = m_g = m$

ultraviolet divergences associated with the different running of α_s above the sparticle threshold. However, this is not the only source of logarithmic behaviour. Since the two-jet cross section does not include final states containing sparticles, there are also infrared divergences when $m^2 \ll s$. Moreover, numerical studies show that the logarithmic asymptotic behaviour does not set in until subenergies beyond the reach of the Fermilab Tevatron collider - for $m = 200$ GeV - or the LHC - for $m = 1$ TeV. For these two reasons, it is not adequate to model the sparticle threshold simply by switching to the above-threshold form of α_s for $s > 4m^2$.

We now use the above results to calculate one-loop corrections to jet cross sections at large E_T and two-jet invariant mass M, by convoluting the above subprocess results with parton distributions. Since the higher-order sparticle corrections are only significant over a small range of parton subenergy in the threshold region, it is convenient to start with the triply-differential cross section as a function of M and the rapidities y_1, y_2 of the final-state jet pair. In terms of the partonic squared matrix elements, this is given by

$$\frac{d^3\sigma}{dM^2 dy_1 dy_2} = \frac{1}{8\pi M^4} \sum_{ijkl} f_i(x_1) f_j(x_2) \left(|\mathcal{M}_{ij}^{kl}(M^2, \hat{t})|^2 + |\mathcal{M}_{ij}^{kl}(M^2, \hat{u})|^2 \right) \tag{4.1}$$

where $f_i(x)$ is the parton distribution function for parton i, $\mathcal{M}_{ij}^{kl}$ is the matrix element for the scattering of parton i and parton j to partons k, l, and the jet rapidities $y_{1,2}$ are given by

$$x_{1(2)} = \frac{M}{\sqrt{s}} e^{\pm(y_1+y_2)}, \tag{4.2}$$

and

$$\hat{t} = -M^2 - \hat{u} = -\frac{M^2}{1 + \exp(y_1 - y_2)}. \tag{4.3}$$

To exemplify the results obtained with (4.1), we consider a number of discrete choices of the jet rapidities $y_{1,2}$, shown in Fig. 7 for the Fermilab Tevatron, and in Fig. 8 for the LHC. We have used the parton-distribution functions

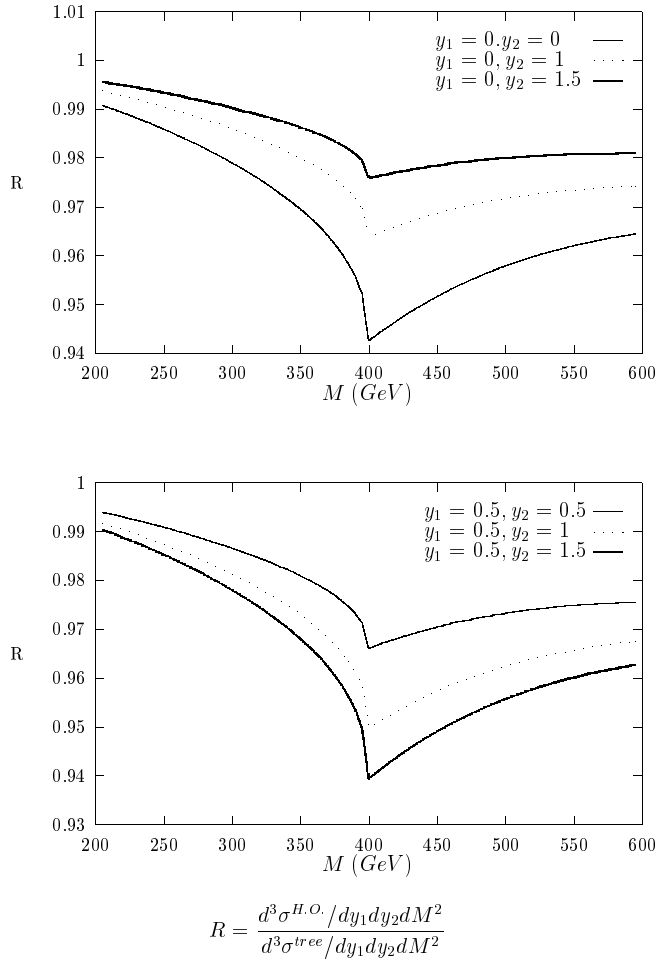

Fig. 7. Triple-differential cross section for $p\bar{p}$ scattering at $\sqrt{s} = 1.8$ TeV, as a function of the two-jet invariant mass M, for various choices of jet rapidities, calculated assuming $m_s = m_g = 200$ GeV. Here and in subsequent plots, R denotes the ratio of the one-sparticle-loop-corrected cross section to the tree-level cross section

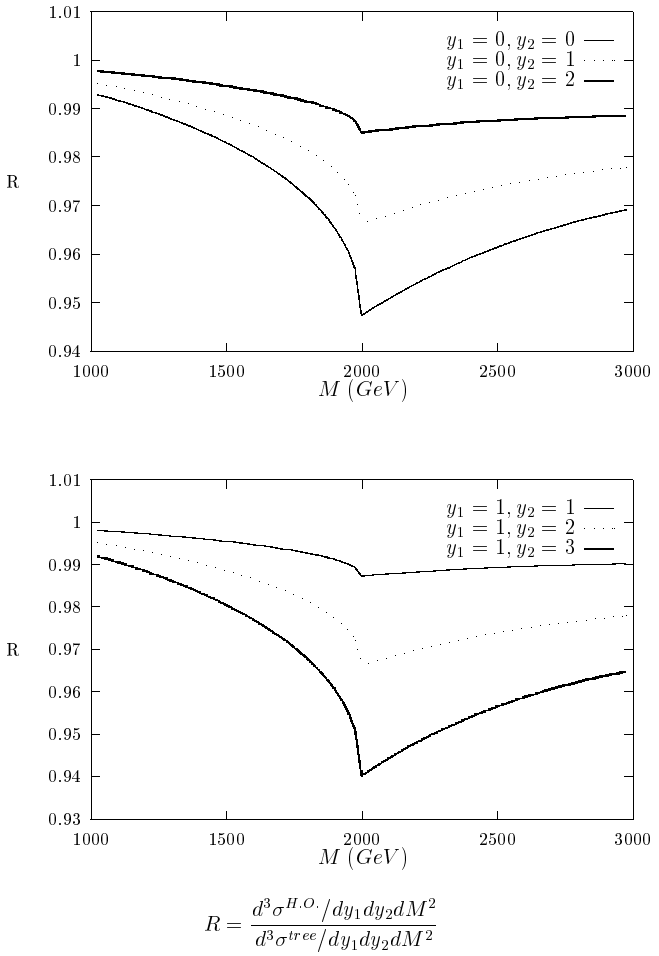

Fig. 8. Triple-differential cross section for pp scattering at $\sqrt{s} = 14$ TeV, as a function of the two-jet invariant mass M, for various choices of jet rapidities, calculated assuming $m_s = m_g = 1$ TeV. Again, R denotes the ratio of the one-sparticle-loop-corrected cross section to the tree-level cross section

from [13], and do not expect that using other parametrizations would significantly affect our results.

The first striking feature is that the corrections are negative. This is because, over most of the ranges of parton momentum fractions x_1, x_2 studied, the subprocesses involving t-channel exchange dominate over the annihilation processes. Indeed, recalling that we must symmetrize over the partons in the final-state jets, we see from the tree-level cross-sections given in [1] that the subprocess cross section for the scattering of two quarks with different flavours at any value of s is *always* an order of magnitude larger than the corresponding cross section for quark-antiquark annihilation, quite apart from the fact that the parton distribution functions provide more flux for this process. The second important feature of the plots shown in Figs. 7,8 is that, although characteristic cusps always appear at threshold, the reduction of the differential cross-section due to the sparticle-loop corrections is significant only for narrow ranges of rapidity pairs, $\{y_1, y_2\}$. For this reason, these corrections are substantially washed out if one integrates over one of the rapidities, in order to obtain the double-differential cross-section, in which the rapidity of only one of the final-state jets is measured. Nevertheless, for sufficiently small values of jet rapidity, there still appears a cusp at threshold, as shown in Fig. 9 for the case of the Fermilab Tevatron collider. However, these cusps are always somewhat diminished and broader than the previous cusps for the triple-differential cross sections. This "washing out" effect is greater for the LHC shown in Fig. 10, where the dip in the threshold region is quite possibly too small to be observed.

This dilution is even more evident in the case of the single-differential cross section as a function of the transverse energy E_T, as shown in Fig. 11 for the case of the Tevatron. There is a broad dip in the cross section for $E_T \simeq m$, but this is probably also too shallow to be observable. This dip is again shallower for the LHC large-E_T cross section, shown in Fig. 12.

In general, the sparticle-loop signal is clearer for sparticles of mass $\simeq 200$ GeV at the Tevatron than for sparticles of mass $\simeq 1$ TeV at the LHC. The reason for this

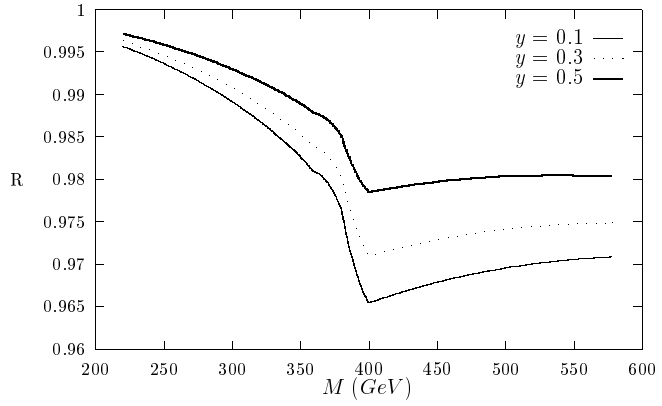

$$R = \frac{d^2\sigma^{H.O.}/dy\,dM^2}{d^2\sigma^{tree}/dy\,dM^2}$$

Fig. 9. Double-differential cross-section for $p\bar{p}$ scattering at $\sqrt{s} = 1.8$ TeV, as a function of the two-jet invariant mass M, for various different jet rapidities, calculated assuming $m_s = m_g = 200$ GeV

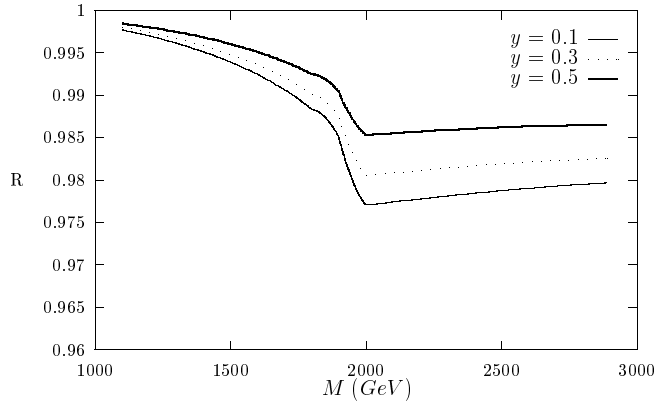

$$R = \frac{d^2\sigma^{H.O.}/dy\,dM^2}{d^2\sigma^{tree}/dy\,dM^2}$$

Fig. 10. Double-differential cross-section for pp scattering at $\sqrt{s} = 14$ TeV, as a function of the two-jet invariant mass M, for various different jet rapidities, calculated assuming $m_s = m_g = 1$ TeV

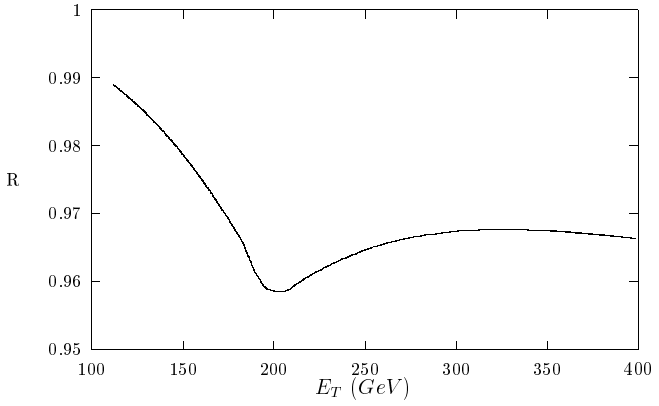

$$R = \frac{d\sigma^{H.O.}/dE_T}{d\sigma^{tree}/dE_T}$$

Fig. 11. Single-differential cross section for $p\bar{p}$ scattering at $\sqrt{s} = 1.8$ TeV, as a function of transverse energy E_T, calculated assuming $m_s = m_g = 200$ GeV

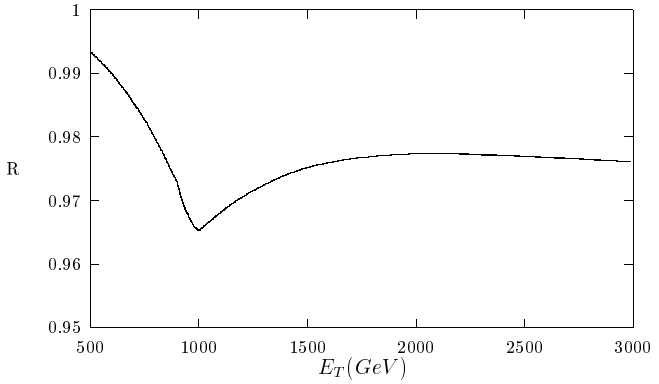

$$R = \frac{d\sigma^{H.O.}/dE_T}{d\sigma^{tree}/dE_T}$$

Fig. 12. Single-differential cross section for pp scattering at $\sqrt{s} = 14$ TeV, as a function of transverse energy E_T, calculated assuming $m_s = m_g = 1$ TeV

is that smaller values of m^2/s are sensitive, on the average, to smaller values of x, thereby sampling more of the gluon content of the incident hadrons. As we saw earlier, the sparticle-loop effects are smallest for purely gluonic scattering. It is, however, noteworthy that the net effect of virtual-sparticle loops is to decrease the predicted cross section, and can therefore not be used even as a partial explanation of any unexpected rise in the large-E_T differential cross section [3].

5 Conclusions

We have presented in this paper complete one-sparticle-loop corrections to the large-E_T and large-M cross sections at high-energy hadron-hadron colliders, and used them to present some numerical results for the Fermilab Tevatron collider and the LHC. We find that the sparticle-loop effects are too small, and of the wrong sign, to make any contribution to explaining the possible large-E_T cross-section discrepancy reported recently [3]. However, the fact that our calculated corrections exhibit cusps at the sparticle threshold may encourage the hope that these effects could be visible in the large-statistics data to be obtained in the future at the Tevatron collider and the LHC.

As we have shown, these cusps are most noticeable in the triple-differential jet cross section $d^3\sigma/dMdy_1dy_2$, and get progressively more washed out as one integrates over one or both jet rapidities, or if one plots the integrated large-E_T cross section. It is for the experimental collaborations to judge whether they will be able to obtain the necessary statistics, and whether the systematic errors can be controlled to the desired low level. In this paper we have

not included any allowance for experimental effects such as the initial transverse momenta of the colliding partons, extra gluon radiation, or the experimental resolution in the large-E_T jet energies.

Evidently, we do not know where the squark and gluino thresholds may be, nor whether they are coincident. The numerical results presented in this paper have been for the optimistic case $m_s = m_g$, and our threshold effects will be surely be spread out and further diluted to some extent if m_s and m_g are substantially different. However, we would like to point out that looking for such a cusps in differential cross sections is in principle a model-independent, though indirect, way of looking for strongly-interacting sparticles. The only vertices that enter our calculations are those proportional to α_s, and the squark and gluino decay vertices do not enter. Thus, looking for the subtle effects we have presented here is a strategy complementary to the direct searches for sparticles decaying according to some particular model scenario, which depends whether R parity conserved or not, and on the spectrum of lighter sparticles. Also, the large cross section for large-E_T jets provides a window on large-mass physics that may reach out to larger sparticle masses than direct searches in specific decay modes with uncertain branching ratios.

Anybody interested in obtaining the code used to derive these results should contact D.A.R., who will make it freely available. J.E. thanks the University of Melbourne School of Physics, and D.A.R. thanks the CERN Theory Division, for hospitality during the completion of this work.

Appendix

In this appendix we list the VP [12] functions used in the text.

Tadpole function

$$\int \frac{d^n k}{(2\pi)^n} \frac{1}{(k^2 - m^2)} = \frac{i}{16\pi^2} A(m) \tag{A.1}$$

Two-point Functions:

$$\int \frac{d^n k}{(2\pi)^n} \frac{1}{(k^2 - m_1^2)((k+p)^2 - m_2)^2} = \frac{i}{16\pi^2} B_0(p^2, m_1^2, m_2^2). \tag{A.2}$$

$$\int \frac{d^n k}{(2\pi)^n} \frac{k^\mu}{(k^2 - m_1^2)((k+p)^2 - m_2)^2} = \frac{i}{16\pi^2} B_1(p^2, m_1^2, m_2^2)\, p^\mu. \tag{A.3}$$

Vertex functions:

$$\int \frac{d^4 k}{(2\pi)^4} \frac{1}{(k^2 - m_1^2)((k+p_1)^2 - m_2)^2((k+p_1+p_2)^2 - m_3^2)} = \frac{i}{16\pi^2} C_0 \tag{A.4}$$

$$\int \frac{d^4 k}{(2\pi)^4} \frac{k^\mu}{(k^2 - m_1^2)((k+p_1)^2 - m_2)^2((k+p_1+p_2)^2 - m_3^2)} = \frac{i}{16\pi^2} \left(C_{11}\, p_1^\mu + C_{12}\, p_2^\mu\right), \tag{A.5}$$

$$\int \frac{d^n k}{(2\pi)^n} \frac{k^\mu k^\nu}{(k^2 - m_1^2)((k+p_1)^2 - m_2)^2((k+p_1+p_2)^2 - m_3^2)} = \frac{i}{16\pi^2} (C_{21}\, p_1^\mu p_1^\nu + C_{22}\, p_2^\mu p_2^\nu + C_{23}(p_1^\mu p_2^\nu + p_2^\mu p_1^\nu) + C_{24} g^{\mu\nu}), \tag{A.6}$$

$$\int \frac{d^n k}{(2\pi)^n} \frac{k^\mu k^\nu k^\rho}{(k^2 - m_1^2)((k+p_1)^2 - m_2)^2((k+p_1+p_2)^2 - m_3^2)} = \frac{i}{16\pi^2} (C_{31}\, p_1^\mu p_1^\nu p_1^\rho + C_{32}\, p_2^\mu p_2^\nu p_2^\rho + C_{33}(p_1^\mu p_1^\nu p_2^\rho + p_1^\mu p_2^\nu p_1^\rho + p_2^\mu p_1^\nu p_1^\rho) + C_{34}(p_1^\mu p_2^\nu p_2^\rho + p_2^\mu p_1^\nu p_2^\rho + p_2^\mu p_2^\nu p_1^\rho) + C_{35}(g_{\mu\nu} p_1^\rho + g_{\mu\rho} p_1^\nu + g_{\nu\rho} p_1^\mu) + C_{36}(g_{\mu\nu} p_2^\rho + g_{\mu\rho} p_2^\nu + g_{\nu\rho} p_2^\mu)), \tag{A.7}$$

where the functions C_0, C_{ij} have in general the arguments $(p_1^2, p_2^2, (p_1+p_2)^2, m_1^2, m_2^2, m_3^2)$. However, in our case we always have $p_1^2 = p_2^2 = 0$, so we suppress the first two arguments.

Box functions:

$$\int \frac{d^4 k}{(2\pi)^4} \times \frac{1}{(k^2 - m_1^2)((k+p_1)^2 - m_2^2)((k+p_1+p_2)^2 - m_3^2)((k-p_4)^2 - m_4^2)} = \frac{i}{16\pi^2} D_0(2p_1\cdot p_2, 2p_2\cdot p_4, m_1, m_2, m_3, m_4), \tag{A.8}$$

$$\int \frac{d^4 k}{(2\pi)^4} \times \frac{k^\mu}{(k^2 - m_1^2)((k+p_1)^2 - m_2^2)((k+p_1+p_2)^2 - m_3^2)((k-p_4)^2 - m_4^2)} = \frac{i}{16\pi^2} D_1(2p_1\cdot p_2, 2p_2\cdot p_4, m_1, m_2, m_3, m_4, \mu), \tag{A.9}$$

$$\int \frac{d^4 k}{(2\pi)^4} \frac{k^\mu k^\nu}{(k^2 - m_1^2)((k+p_1)^2 - m_2^2)((k+p_1+p_2)^2 - m_3^2)((k-p_4)^2 - m_4^2)} = \frac{i}{16\pi^2} D_2(2p_1\cdot p_2, 2p_2\cdot p_4, m_1, m_2, m_3, m_4, \mu, \nu), \tag{A.10}$$

$$\int \frac{d^4k}{(2\pi)^4} \times \frac{k^\mu k^\nu k^\rho}{(k^2-m_1^2)((k+p_1)^2-m_2^2)((k+p_1+p_2)^2-m_3^2)((k-p_4)^2-m_4^2)} = \frac{i}{16\pi^2} D_3(2p_1\cdot p_2, 2p_2\cdot p_4, m_1, m_2, m_3, m_4, \mu, \nu, \rho), \tag{A.11}$$

$$\int \frac{d^nk}{(2\pi)^n} \times \frac{k^\mu k^\nu k^\rho k^\sigma}{(k^2-m_1^2)((k+p_1)^2-m_2^2)((k+p_1+p_2)^2-m_3^2)((k-p_4)^2-m_4^2)} = \frac{i}{16\pi^2} D_4(2p_1\cdot p_2, 2p_2\cdot p_4, m_1, m_2, m_3, m_4, \mu, \nu, \rho, \sigma). \tag{A.12}$$

For the sake of compactness, we do not write these tensor expressions out in terms of the vectors $p_1 \cdots p_4$, but refer the reader to [12] for details.

The exact forms of the functions B_i, C_i, C_{ij}, D_i are given in [12]. The functions $A, B_0, B_1, C_{24}, C_{35}, C_{36}, D_4$ are ultraviolet divergent, and therefore should be calculated in $n = 4 - 2\epsilon$ dimensions. The pole parts of these functions are given by the following expressions:

$$\text{P.P}\{A(m)\} = \frac{m^2}{\epsilon} \tag{A.13}$$

$$\text{P.P}\{B_0(x, m_1, m_2)\} = \frac{1}{\epsilon} \tag{A.14}$$

$$\text{P.P}\{C_{24}(x, m_1, m_2, m_3)\} = \frac{1}{4\epsilon} \tag{A.15}$$

$$\text{P.P}\{C_{35}(x, m_1, m_2, m_3)\} = -\frac{1}{6\epsilon} \tag{A.16}$$

$$\text{P.P}\{C_{36}(x, m_1, m_2, m_3)\} = -\frac{1}{12\epsilon} \tag{A.17}$$

$$\text{P.P}\{D_4(x, y, m_1, m_2, m_3, m_4, \mu, \nu, \rho, \sigma)\} = \frac{1}{24\epsilon}\left(g^{\mu\nu}g^{\rho\sigma} + g^{\mu\rho}g^{\nu\sigma} + g^{\mu\sigma}g^{\nu\rho}\right) \tag{A.18}$$

References

1. R.K. Ellis and J. Sexton, Nucl. Phys. **B269** (1986) 445
2. Z. Kunszt and D. Soper, Phys. Rev. **D46** (1992) 192
3. CDF Collaboration, F. Abe et al., Phys. Rev. Lett. **77** (1996) 438, 5336
4. F. Nang, for the CDF and D0 collaborations, Fermilab preprint CONF-97-192-E; D0 Collaboration, S. Abachi et. al., Fermilab preprint PUB-97-237-E, hep-ex/9707016
5. J. Huston, E. Kovacs, S. Kuhlmann, H.L. Lai, J.F. Owens, D. Soper and W.K. Tung, Phys. Rev. Lett. **77** (1996) 444; H.L. Lai, J. Huston, S. Kuhlmann, F. Olness, J. Owens, D. Soper, W.K. Tung and H. Weerts, Phys. Rev. **D55** (1997) 1280; S. Kuhlmann, H.L. Lai and W.K. Tung, hep-ph/9704338; for a review, see W.K. Tung, hep-ph/9608293
6. E.W.N. Glover, A.D. Martin. R.G. Roberts and W.J. Stirling, Phys. Lett. **B381** (1996) 353; for a review, see W.J. Stirling, hep-ph/9608411
7. V. Barger, M.S. Berger and R.J.N. Phillips, Phys. Lett. **B382** (1996) 178
8. P. Kraus and F. Wilczek, Phys. Lett. **B382** (1996) 262
9. for a review, see W. Hollik, hep-ph/9703231
10. J. Ellis and D.A. Ross, Phys. Lett. **B383** (1996) 187
11. C.S. Kim and S. Alam, Phys. Lett. **B398** (1997) 110
12. G. Passarino and M. Veltman, Nucl. Phys. **B160** (1979) 151
13. A.D. Martin, R.G. Roberts, W.J. Stirling, Phys. Lett. **B387** (1996) 419